X-ray–Induced Dissociation of H2O and Formation of an O 2–H2 Alloy at High Pressure

Wendy L. Mao, *et al.*

Science **314**, 636 (2006);
DOI: 10.1126/science.1132884

Science (print ISSN 0036-8075; online ISSN 1095-9203) is published weekly, except the last week in December, by the American Association for the Advancement of Science, 1200 New York Avenue NW, Washington, DC 20005.

X-ray–Induced Dissociation of H_2O and Formation of an O_2–H_2 Alloy at High Pressure

Wendy L. Mao,[1] Ho-kwang Mao,[2,3] Yue Meng,[3] Peter J. Eng,[4] Michael Y. Hu,[3] Paul Chow,[3] Yong Q. Cai,[5] Jinfu Shu,[2] Russell J. Hemley[2]

When subjected to high pressure and extensive x-radiation, water (H_2O) molecules cleaved, forming O–O and H–H bonds. The oxygen (O) and hydrogen (H) framework in ice VII was converted into a molecular alloy of O_2 and H_2. X-ray diffraction, x-ray Raman scattering, and optical Raman spectroscopy demonstrated that this crystalline solid differs from previously known phases. It remained stable with respect to variations in pressure, temperature, and further x-ray and laser exposure, thus opening new possibilities for studying molecular interactions in the hydrogen-oxygen binary system.

H_2O forms at least 15 stable (*1*) and metastable crystalline (*2*–*5*) and amorphous ices (*6*–*9*). Its rich phase diagram displays a range of exotic behavior such as symmetric hydrogen bonds (*10*–*12*), superionic ice (*13*, *14*), and multiple critical points (*15*, *16*). We excited H_2O with high-energy x-radiation to access a larger portion of the energy landscape at high pressure. Although at ambient pressure x-rays are known to produce metastable free radicals in molecular systems or to induce stable reactions by overcoming kinetic-energy barriers, documented examples of x-ray–induced transitions at high pressure have been extremely rare.

We observed the x-ray– and pressure-induced cleaving of H_2O in an oxygen K-edge study with a high-pressure x-ray Raman scattering (XRS) technique (*5*, *17*–*19*) that requires long exposure of moderately high energy (~10-keV) x-radiation. For oxygen bonded with hydrogen in H_2O, the K-edge XRS spectra are dominated by a cluster of peaks around 540 eV, as shown in dense water below 0.9 GPa, ice VI between 1 and 2 GPa, and ice VII just above 2 GPa (Fig. 1). At pressures above 2.5 GPa, however, x-radiation induced pronounced, irreversible changes in the XRS spectra. A distinctive, sharp peak appeared at 530 eV that was characteristic of O–O bonding in O_2 and grew with time, reaching a plateau after 6 hours of exposure to the incident x-ray beam (Fig. 1). The plateau intensity increased with increasing pressure, and at 15.3 GPa, the height of the 530-eV peak matched that of the main 540-eV multiplet. We observed the reaction independently at the Advanced Photon Source (APS) and at SPring-8 during high-pressure XRS measurements of H_2O (Fig. 1). Visually, the sample changed from colorless to light brown after the conversion (Fig. 2A). Optical Raman scattering (ORS) measurements showed intense, characteristic H_2 and O_2 vibrons and a diminished H_2O signal (Fig. 3), clearly demonstrating the dissociation of H_2O molecules and the recombination into O_2 and H_2 molecules.

The resultant O_2 and H_2 molecules did not exist in the known high-pressure phases of hexagonal close-packed (hcp)–H_2 and ε-O_2 but formed an alloy consisting of both molecular O_2 and H_2. To better understand this material, we varied x-ray energy and exposure time, interval between exposure and measurement, pressure, and temperature, and we studied the samples with ORS and x-ray diffraction (XRD). At 17.6 GPa after x-radiation, the OH vibrational modes around 3000 cm^{-1} became diminishingly weak and exhibited a different shape in comparison to that of ice VII (Fig. 3), indicating that the H_2O molecules had mostly cleaved, leaving only a minor component in the new O_2–H_2 alloy. We can rule out the hcp-H_2 and ε-O_2 phases on the basis of their characteristic ORS spectra. The intense $Q_1(1)$ H_2 molecular vibron at 4304 cm^{-1} (Fig. 3) is 59 cm^{-1} above the $Q_1(1)$ of pure hcp-H_2 (4245 cm^{-1}) (*20*). The weak side peak at 4236 cm^{-1} indicates a small amount (<5%) of H_2 in a different site or possibly in a new secondary phase. The H_2 molecular excitations [$S_0(0)$, $S_0(1)$, and $S_0(2)$ at 360, 610, and 847 cm^{-1}, respectively] are characteristic of freely rotating H_2 molecules. The O_2 ORS vibron frequency (1577 cm^{-1}) is similar to that of ε-O_2 (*21*, *22*), but the intense, low-frequency, librational peaks

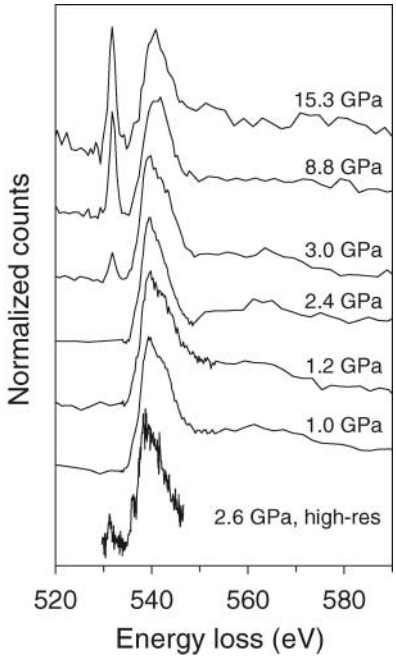

Fig. 1. XRS of the H_2O sample at high pressure after 12 hours of irradiation. The bottom spectrum at 2.6 GPa was measured at beamline BL12XU, SPring-8, by means of 9.886-keV x-radiation with high-energy resolution (300 meV). All other spectra for 1.0, 1.2, 2.4, 3.0, 8.8, and 15.3 GPa were measured with 9.687-keV x-radiation at beamline 13-IDC, APS, ANL, with 1-eV resolution.

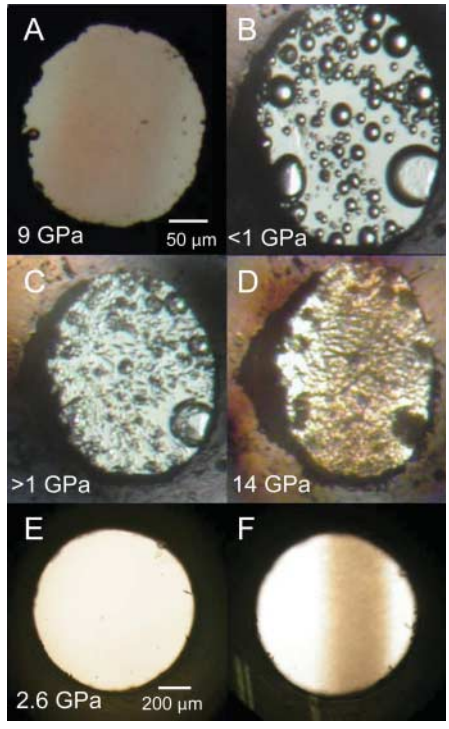

Fig. 2. Photomicrographs of two diamond anvil cell samples. The top four panels were taken at 13-IDC, APS, ANL; the bottom two panels were taken at BL12XU, SPring-8. (**A**) Sample after XRS measurement at 8.8 GPa. The light brown streak through the middle of the sample shows the portion irradiated by the x-ray beam. A small ruby ball on the left edge of the gasket was used for pressure calibration. (**B**) After the release of pressure to below 1 GPa, bubbles of O_2 and H_2 formed. (**C**) Bubbles collapsed upon the increase of pressure as the H_2 and O_2 were incorporated into the crystalline sample. (**D**) Sample after XRS measurement at 15.3 GPa. (**E**) Sample before and (**F**) after x-ray exposure at 2.6 GPa.

[1]Los Alamos Neutron Science Center, Los Alamos National Laboratory, Los Alamos, NM 87545, USA. [2]Geophysical Laboratory, Carnegie Institution of Washington, Washington, DC 20015, USA. [3]High Pressure Collaborative Access Team, Carnegie Institution of Washington, Advanced Photon Source, Argonne National Laboratory, Argonne, IL 60439, USA. [4]Consortium for Advanced Radiation Sources, University of Chicago, Chicago, IL 60637, USA. [5]National Synchrotron Radiation Research Center, Hsinchu 30076, Taiwan.

at 123 and 272 cm^{-1} are substantially lower in frequency than the characteristic ν_{L1} and ν_{L2} modes of ε-O_2 at 155 and 360 cm^{-1}, respectively, indicating that this phase is not ε-O_2. The observation of a single O_2 vibron and a predominant H_2 vibron is consistent with a new alloy conserving the O_2:H_2 ratio of approximately 1:2 [i.e., $(O_2)(H_2)_2$], although we cannot rule out the possibility of a minor secondary phase with a different O_2:H_2 ratio, corresponding to the weak H_2 side peak at 4236 cm^{-1}.

The H_2 vibron stiffening in mixed crystals has been used extensively to reveal information on the matrix isolation and intermolecular interactions of H_2 (*23*, *24*). The vibron turnover of pure hcp-H_2 (*20*) shifts to higher pressure in the mixed crystals, and the effect increases with increasing molecular fraction of other molecules, such as Ne, HD, and D_2 (*23*, *24*). In the transformed material, the main H_2 vibron shows substantial stiffening, which suggests the presence of a large amount of O_2 (Fig. 3). The pressure shifts of the ORS O_2 librational peaks and H_2 vibrons are shown in Fig. 4 and are compared with corresponding peaks of hcp-H_2 and ε-O_2. Similar pressure dependence and constant offset of ORS peaks of the present alloy with respect to the pure endmembers indicate that these peaks have similar origins but different matrices' effects.

We conducted XRD studies of the H_2–O_2 alloy at beamline 16-IDB of the High Pressure Collaborative Access Team (HPCAT), APS, Argonne National Laboratory (ANL). Sharp powder diffraction rings indicate that the alloy is a well-crystallized solid. Its diffraction pattern (Fig. 5) shows some similarity to, but does not exactly fit, ε-O_2 (*25*–*27*). For instance, they both have a multiplet group between 2 and 2.4 Å, and the alloy has a doublet near 3.4 Å, where ε-O_2 has a singularly strong peak (*25*). At this point, it is premature to present a definitive crystal structure or unit cell based on only 10 powder XRD lines. The *d*-spacings of the alloy, ε-O_2, and ice VII vary similarly with pressure, implying that all have similar compressibilities (Fig. 6).

Once synthesized and kept at high pressure, the new phase was stable with respect to laser exposure, further x-radiation, and being stored for time intervals of more than 120 days. Bubbles of O_2–H_2 gaseous mixture (identified by ORS) were released from the solid when the pressure was reduced below 1 GPa (Fig. 2B). When these bubbles were compressed to high pressures and irradiated with x-rays again, they re-formed the new alloy (Fig. 2D). Formation of this material has thus been approached from both directions, starting with H_2O and with an O_2–H_2 mixture. Heated in a diamond anvil cell, the alloy is stable up to 700 K at 15 GPa. At higher temperatures, this material reverts to ice VII near melting.

Partial dissociation of ice VII was previously observed by Lin *et al*. (*28*) in high pressure–high temperature experiments of H_2O, but the reaction conditions and products were different. At high temperature and without x-radiation, Lin *et al*. detected a minor amount of ε-O_2 (but no H_2) as a result of hydrogen loss to the metal gasket. The present observation also differs from results for hydrogen peroxide (H_2O_2), which when compressed, first transforms to a high-pressure phase (H_2O_2-II) and then at high pressures decomposes to H_2O + O_2, without the production of any H_2 molecules (*29*). Our alloy does not match the $(O_2)_3(H_2)_4$ phase reported at 7.5 to 10 GPa (*30*), which was unstable and combusted during x-radiation. Moreover, the O_2 and H_2 ORS vibrons of the $(O_2)_3(H_2)_4$ phase agree with those of ε-O_2 and hcp-H_2, respectively, and thus differ from those of our alloy.

The kinetic stability of the new material implies that there is an energy minimum separated from ice VII by a large energy barrier. The barrier may be too high to cross by thermal excitation alone, because it has not been observed in high pressure–high temperature experiments up to 1000 K (*14*, *28*), which is equivalent to 0.08 eV. The ~10-keV x-rays that we used provide access to a large range of local energy minimum states, including both ground and trapped excited electronic states of O_2 and H_2. It may be puzzling why this new phase was not discovered earlier in previous XRD studies of high-pressure ices. We conducted a reconnaissance study using several different monochromatic x-ray

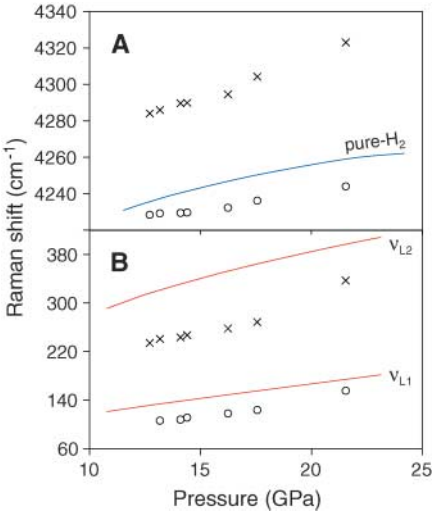

Fig. 4. Pressure dependence of ORS shift for the O_2–H_2 alloy. (**A**) Symbols show the positions for the H_2 vibron doublet. Blue line shows the position for the pure H_2 vibron (*20*). (**B**) Symbols show the positions of the low frequency modes. Red lines show the librational modes of ε-O_2 (*21*, *22*).

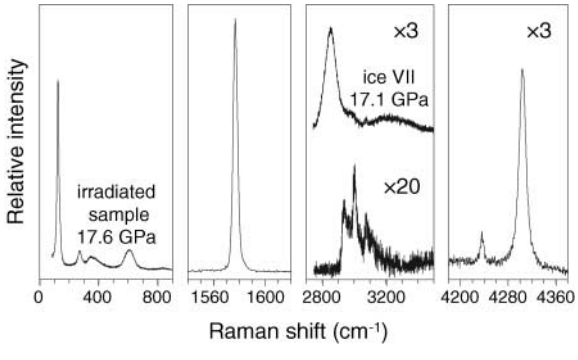

Fig. 3. ORS measurements of an irradiated sample at 17.6 GPa. The ORS measurements of an unirradiated ice VII sample at 17.1 GPa are shown for comparison. All measurements were based on the same exposure time; intensity scaling is noted by multiplication factors. The Raman modes in the sample were excited using Ar^+ ion laser radiation at 488 nm.

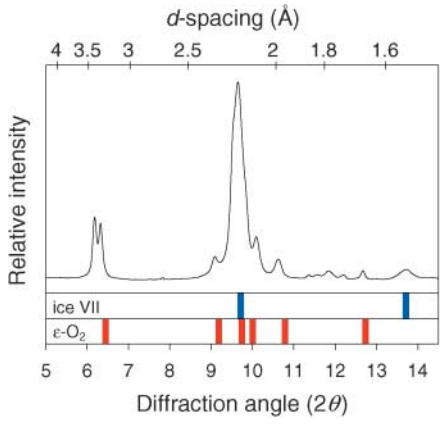

Fig. 5. Integrated XRD pattern of the irradiated sample at 15.3 GPa, where wavelength λ = 0.36819 Å. Comparisons for expected peak positions at 15.3 GPa for ε-O_2 (*21*, *26*) and ice VII (*31*) at 15.3 GPa are shown as red and blue bars, respectively.

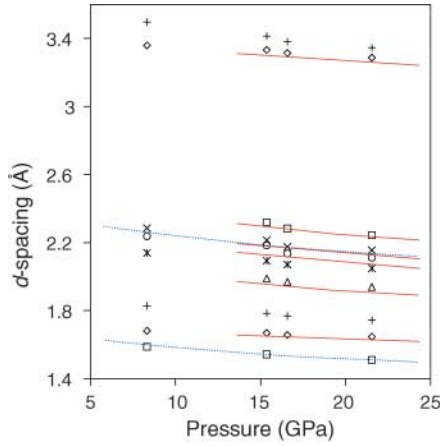

Fig. 6. Pressure dependence of *d*-spacings for reflections from the new O_2–H_2 alloy. Solid red and dotted blue lines show the pressure dependence for ε-O_2 (*21*, *26*) and ice VII (*31*), respectively.

energies of 9.687, 9.886, 14.414, and 33.678 keV. The x-ray–induced reaction in ice VII was most effective with 9.687- and 9.886-keV x-radiation, which are absorbed readily by H_2O; was less effective with 14.414-keV x-radiation; and was not observed with 33.678-keV high-energy x-radiation, which passed through H_2O without adequate absorption. High-pressure synchrotron XRD studies typically use high-energy x-radiation above 20 keV with short exposure times of seconds to minutes; this would be insufficient to induce the reaction. On the other hand, low-energy x-radiation below 12 keV would be largely absorbed by the diamond anvils and are seldom used for XRD studies. In our experiments, the ~10-keV x-rays pass through the low-absorbance Be gasket and provide optimal conditions for inducing the reaction.

References and Notes

1. V. F. Petrenko, R. W. Whitworth, *Physics of Ice* (Oxford Univ. Press, New York, 1999).
2. I.-M. Chou *et al.*, *Science* **281**, 809 (1998).
3. C. Lobban, J. L. Finney, W. F. Kuhs, *Nature* **391**, 268 (1998).
4. J. S. Tse, D. D. Klug, *Phys. Rev. Lett.* **81**, 2466 (1998).
5. Y. Q. Cai *et al.*, *Phys. Rev. Lett.* **94**, 025502 (2005).
6. O. Mishima, L. D. Calvert, E. Whalley, *Nature* **310**, 393 (1984).
7. R. J. Hemley, L. C. Chen, H. K. Mao, *Nature* **338**, 638 (1989).
8. J. L. Finney *et al.*, *Phys. Rev. Lett.* **88**, 225503 (2002).
9. C. A. Tulk *et al.*, *Science* **297**, 1320 (2002).
10. A. F. Goncharov, V. V. Struzhkin, M. S. Somayazulu, R. J. Hemley, H. K. Mao, *Science* **273**, 218 (1996).
11. M. Bernasconi, P. L. Silvestrelli, M. Parrinello, *Phys. Rev. Lett.* **81**, 1235 (1998).
12. A. F. Goncharov, V. V. Struzhkin, H. K. Mao, R. J. Hemley, *Phys. Rev. Lett.* **83**, 1998 (1999).
13. C. Cavazzoni *et al.*, *Science* **283**, 44 (1999).
14. A. F. Goncharov *et al.*, *Phys. Rev. Lett.* **94**, 125508 (2005).
15. O. Mishima, H. E. Stanley, *Nature* **396**, 329 (1998).
16. L. Liu *et al.*, *Phys. Rev. Lett.* **95**, 117802 (2005).
17. W. L. Mao *et al.*, *Science* **302**, 425 (2003).
18. Y. Meng *et al.*, *Nat. Mater.* **3**, 111 (2004).
19. S. K. Lee *et al.*, *Nat. Mater.* **4**, 851 (2005).
20. S. K. Sharma, H. K. Mao, P. M. Bell, *Phys. Rev. Lett.* **44**, 886 (1980).
21. Y. A. Freiman, H. J. Jodl, *Phys. Rep.* **401**, 1 (2004).
22. Y. Akahama, H. Kawamura, *Phys. Rev. B* **54**, R15602 (1996).
23. P. Loubeyre, R. Letoullec, J. P. Pinceaux, *Phys. Rev. Lett.* **67**, 3271 (1991).
24. D. M. Brown, W. B. Daniels, *Phys. Rev. A.* **45**, 6429 (1992).
25. H. Fujihisa *et al.*, *Phys. Rev. Lett.* **97**, 085503 (2006).
26. Y. Akahama *et al.*, *Phys. Rev. Lett.* **74**, 4690 (1995).
27. G. Weck, P. Loubeyre, R. LeToullec, *Phys. Rev. Lett.* **88**, 035504 (2002).
28. J.-F. Lin *et al.*, *Geophys. Res. Lett.* **32**, L11306 (2005).
29. H. Cynn, C. S. Yoo, S. A. Sheffield, *J. Chem. Phys.* **110**, 6836 (1999).
30. P. Loubeyre, R. LeToullec, *Nature* **378**, 44 (1995).
31. Y. Fei, H. K. Mao, R. J. Hemley, *J. Chem. Phys.* **99**, 5369 (1993).

32. We thank S. Ghosh for assistance with the XRS at APS; N. Hiraoka, I. Jarrige, H. Ishii, and C. C. Chen for assistance with the XRS at SPring-8; S. Sinogeiken for assistance with the ORS; and M. Somayazulu and A. Levedahl for assistance with resistive heating measurements. The NSF–Division of Materials Research (DMR-0508988), NSF–Division of Earth Sciences (EAR) Petrology and Geochemistry, NSF-EAR Geophysics, and NSF-EAR Instrumentation and Facility Programs provided financial support, and HPCAT provided synchrotron beam time. GeoSoilEnviro Consortium for Advanced Radiation Sources is supported by the NSF-EAR (EAR-0217473), U.S. Department of Energy (DOE)–Geosciences (DE-FG02-94ER14466), and State of Illinois. HPCAT is supported by the DOE–Basic Energy Sciences (BES), DOE–National Nuclear Security Administration, Carnegie DOE Alliance Center, NSF, Department of Defense–Tank-Automotive and Armaments Command, and W. M. Keck Foundation. APS is supported by the DOE-BSE, Office of Energy Research, under contract W-31-109-Eng-38. The work performed at BL12XU, SPring-8, is partly supported by the National Synchrotron Radiation Research Center and National Science Center of Taiwan.

21 July 2006; accepted 14 September 2006
10.1126/science.1132884

Colloid Transport of Plutonium in the Far-Field of the Mayak Production Association, Russia

Alexander P. Novikov,[1] Stepan N. Kalmykov,[1,2] Satoshi Utsunomiya,[3] Rodney C. Ewing,[3]* François Horreard,[4] Alex Merkulov,[4] Sue B. Clark,[5] Vladimir V. Tkachev,[1] Boris F. Myasoedov[1]

Sorption of actinides, particularly plutonium, onto submicrometer-sized colloids increases their mobility, but these plutonium colloids are difficult to detect in the far-field. We identified actinides on colloids in the groundwater from the Mayak Production Association, Urals, Russia; at the source, the plutonium activity is ~1000 becquerels per liter. Plutonium activities are still 0.16 becquerels per liter at a distance of 3 kilometers, where 70 to 90 mole percent of the plutonium is sorbed onto colloids, confirming that colloids are responsible for the long-distance transport of plutonium. Nano–secondary ion mass spectrometry elemental maps reveal that amorphous iron oxide colloids adsorb Pu(IV) hydroxides or carbonates along with uranium carbonates.

Submicrometer-sized colloids, consisting of inorganic and/or organic compounds, occur at up to 10^{17} particles per liter in groundwater and provide an important means of transporting elements with low solubilities, including the actinides (*1*–*3*). The stability of these colloids is a function of the composition of groundwater and the hydrologic conditions (*4*).

The formation of actinide pseudo-colloids, in which the actinide sorbs onto aquatic colloids, can stabilize actinides in natural waters and increase their concentrations by many orders of magnitude over the values expected from solubility calculations (*2*, *5*). The association of Pu with colloids 25 to 450 nm in size has been observed 3.4 km from a source at Los Alamos National Laboratory (*6*). This migration distance is greater than modeled estimates (*7*). Similar transport has also been seen at the Savannah River Site (*8*). At Nevada Test Site, Pu has migrated 1.3 km in 30 years in groundwater by means of colloids with sizes of 7 nm to 1 μm (*9*). Model results imply that colloid-facilitated transport of actinides at Yucca Mountain could lead to as much as a 60-fold increase in the total effective dose equivalent to an exposed population (*10*).

Colloid-facilitated transport is likely the means for actinides' long-distance transport in groundwater. Many previous studies have experimentally demonstrated adsorption of Pu onto a variety of minerals and mineral assemblage (*11*–*13*). However, little is known of the speciation of the actinides or the type of colloids with which they are associated, particularly during the transport in the far-field where there are many competing processes, such as desorption from the colloids and resorption onto minerals.

To understand the colloid-associated actinides and their long-distance transport in groundwater, we investigated Pu migration in the natural groundwater system at one of the most contaminated nuclear sites in the world: Mayak, Russia. Mayak is a nuclear waste reprocessing plant near Kyshtym, in the Southern Urals, Russia (*14*) (Fig. 1). Waste effluents containing ^{90}Sr, ^{137}Cs, ^{241}Am, and ^{239}Pu were discharged into Lake Karachai (*15*, *16*); these were weakly alkaline $NaNO_3$ brine solutions with a pH of 7.9 to 9.3 and a salt concentration of 16 to 145 g/liter. The major dissolved ionic species were NO_3^- (11 to 78 g/liter), CH_3COO^- (0.6 to 20 g/liter), $C_2O_4^{2-}$ (0.9 to 14 g/liter), SO_4^{2-} (0.12 to 1.3 g/liter), Na^+ (6 to 32 g/liter), Cl^- (20 to 350 mg/liter), U(VI) (13 to 196 mg/liter), Ca^{2+} (8 to 80 mg/liter), and

[1]Vernadsky Institute of Geochemistry and Analytical Chemistry, Russian Academy of Sciences, Moscow 119991, Russia. [2]Radiochemistry Division, Chemistry Department, Lomonosov Moscow State University, Moscow 119992, Russia. [3]Department of Geological Sciences, University of Michigan, Ann Arbor, MI 48109–1005, USA. [4]Cameca, 92622 Gennevilliers Cedex, 92403, France. [5]Department of Chemistry and Nuclear Radiation Center, Washington State University, Pullman, WA 99164–4630, USA.

*To whom correspondence should be addressed. E-mail: rodewing@umich.edu